Pressure Induced Enlargement and Ionic Current Rectification in Symmetric Nanopores

Sebastian J. Davis,[†] Michal Macha,[†] Andrey Chernev,[†] David M. Huang,[‡] Aleksandra Radenovic,[†] and Sanjin Marion[*,†]

†*Laboratory of Nanoscale Biology, Institute of Bioengineering, School of Engineering, EPFL, 1015 Lausanne, Switzerland*

‡*Department of Chemistry, School of Physical Sciences, The University of Adelaide, Adelaide, Australia*

E-mail: sanjin.marion@epfl.ch,aleksandra.radenovic@epfl.ch

Abstract

Nanopores in solid state membranes are a tool able to probe nanofluidic phenomena, or can act as a single molecular sensor. They also have diverse applications in filtration, desalination, or osmotic power generation. Many of these applications involve chemical, or hydrostatic pressure differences which act on both the supporting membrane, and the ion transport through the pore. By using pressure differences between the sides of the membrane, and an alternating current approach to probe ion transport, we investigate two distinct physical phenomena: the elastic deformation of the membrane through the measurement of strain at the nanopore, and the growth of ionic current rectification with pressure due to pore entrance effects. These measurements are a significant step towards the understanding of the role of elastic membrane deformation or fluid flow on linear and non-linear transport properties of nanopores.

Keywords

nanopore, strain, pressure, enlargement, ionic current rectification, nanofluidics

Introduction

Nanopores are a single molecule tool with diverse applications in bio-sensing,[1,2] osmotic power generation,[3] and water desalination.[4] A nanoscale pore separates two reservoirs filled with electrolyte. Monitoring ion transport through the pore yields information about a passing analyte such as DNA, or on non-linear phenomena such as ionic current rectification (ICR)[5] and other nanofluidic effects.[6–8] Solid state nanopores are readily made in silicon nitride suspended membranes since they are compatible with standard lithography techniques. Pores in these suspended membranes can be used as such, as in this study, or can further support a membrane made of quasi-2D materials such as molybdenum disulphide, hexagonal boron nitride, or graphene in which a small pore can be further drilled.[9,10]

The combination of hydrostatic pressure gradients with nanopores has so far been mostly used to modify analyte translocations,[11–14] the surface charge of the pore,[15] or as a tool to control wetting.[16]. It has been shown that pressure can strongly influence the ion transport properties of a nanopore or nanochannel depending on the system's resistance to hydraulic fluid flow, and modulate ion transport.[17,18] On the other hand, ICR,[7] which is linked to ion selectivity, has been found to be reduced in conical pores under the influence of pressure induced fluid flow.[19,20]

The application of pressure on thin supported membranes is a well-established technique for studying the elastic properties of thin films. Blistering of thin membranes such as silicon nitride,[21] or blistering and delamination of 2D materials[22–24] has been extensively studied in dry conditions. Studies in liquid and with nanopores have so far been restricted to nanopores drilled in elastomeric membranes for studying analyte translocations.[25,26] No experiments have been performed to date with nanopores in elastic solid-state membranes, although such

membranes are usually used in conditions of osmotic or hydraulic pressure gradients which could influence pore properties like ion selectivity and water permeability.[3,4,27] Theoretical work on sub-nm pores in 2D materials indicates the presence of strong mechanosensitivity to lateral stresses.[28–32] To realize a truly mechanosensitive solid-state sensor, one which would mimic mechanosensitive biological channels,[33] one needs to first understand the elastic behaviour of nanopores in solid state membranes.

This study aims to quantify the role of hydraulic pressure in modulating ion transport in thin, symmetrical, charged nanopores using a phase sensitive amplifier enhancing the sensitivity. We decouple two independent physical phenomena. First, that the pressure induced deformation of the supporting membrane causes an enlargement in the nanopore size. This allows direct measurement of the local membrane stress in a liquid environment as a precursor for stressing 2D material nanopores and probing mechanosensitivity.[29] Secondly, we demonstrate that pressure induced-fluid flow produces ICR despite the lack of the usually required geometrical asymmetry in the pore[5,7] or asymmetric buffer conditions such as concentration or viscosity.[34,35] This is opposite to the so far reported role of pressure in reducing ICR in asymmetrical nanopores.[19,20] These results are therefore key in furthering the understanding of the effect of membrane elastic deformations or fluid flow on the transport properties of nanopores.

Pressure application experimental setup

To study how hydrostatic pressure and potential differences influence the ion transport through a solid state nanopore we use a sealed, pressure-tight chamber (See Materials and Methods and Figure 1a) as described previously.[16] After a sample consisting of a membrane with an 80 nm diameter nanopore is mounted into the chamber, the system is wetted with a degassed 1 M KCL buffered solution under 7 bar compression pressure. Pressure P is applied using a microfluidics pressure controller. Positive pressure is defined as being ap-

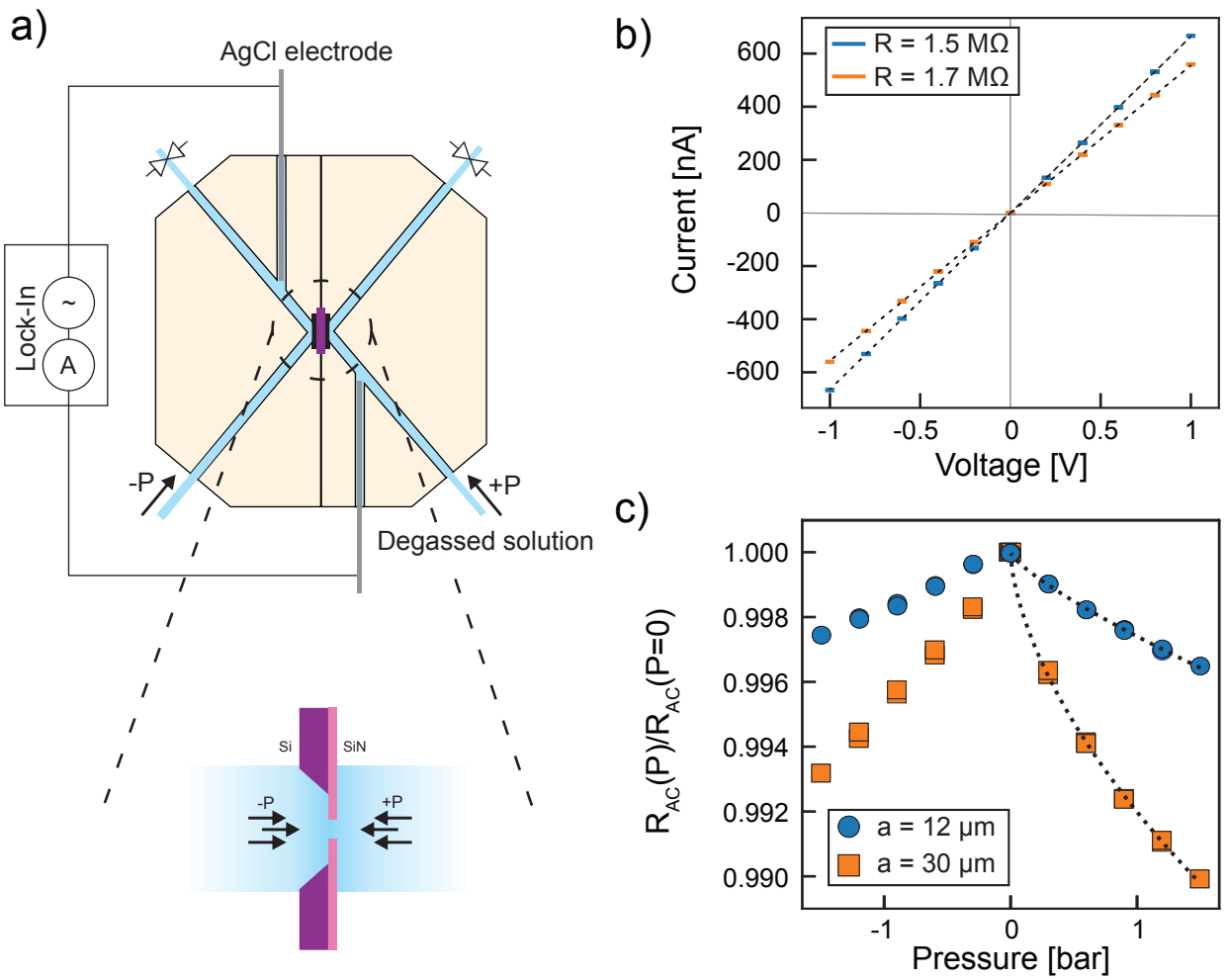

Figure 1: **Application of pressure to solid state nanopores. a)** Schematic in side view of the sealed pressure chamber channels and electrical measurement. Zoom below shows the chip area and the convention of pressure sign. **b)** DC IV curves for two representative samples having different square membrane sizes (a = 12 μm and 30 μm) but similar pore sizes of $d_0 \approx 80$ nm. Lines are linear fits giving resistance values of 1.5 MΩ and 1.7 MΩ. **c)** Mean values of resistance R_{AC} as a function of pressure normalized by the value of the resistance under no pressure $R_{AC}(P = 0)$. The curves represent the same samples as in panel (b). Lines are a fit to eq. 2 without residual stress giving $a = 12.8 \pm 1.0$ μm, and $a = 30.6 \pm 6.2$ μm respectively.

plied from the front-side of the membrane (flat side), and negative pressure as being applied from the back-side (etch-side) (as seen on Figure 1a). A potential difference V between the two sides of the membrane is applied and read with Ag/AgCl electrodes. Measurements of current I versus applied potential V are shown on Figure 1b. Only samples showing stable conductance and current noise levels were considered for further analysis (See Supporting information Sec. S2).

The current response of the nanopore to an external potential difference V, and a pressure difference P between the two sides of the membrane is of the form $I = G(V,P)V + H_s P$, where H_s is the streaming conductance, and $G(V,P)$ the electrical conductance. The non-linearity in conductance being almost negligible (Figure 1b), we perform a Taylor expansion of the conductance $G(V,P) \approx G_1(P) + G_2(P)V$, with G_1 and G_2 corresponding to the linear and first non-linear contribution.[16] The conductance term G_1 has contributions from the pore interior, and the access region resistance and obeys $G_1 = \Lambda \left[4L/\pi d^2 + 1/d\right]^{-1}$, where d is the diameter of the nanopore, L the thickness of the membrane, and Λ the bulk conductance of the solution.[36,37] One measure of the non-linearity in ion transport is the ICR ratio[5,7] which we define as:

$$r(V,P) = \frac{|I(+V,P) - I(V=0,P)|}{|I(-V,P) - I(V=0,P)|} \approx \frac{G_1(P) + G_2(P)|V|}{G_1(P) - G_2(P)|V|}, \tag{1}$$

to exclude any streaming contribution.

In order to deconvolute the linear and non-linear ion transport contributions of the nanopore, and eliminate any streaming current contribution, we perform all measurements using a quasi-static AC measurement. All AC measurements are performed using a sinusoidal voltage at a frequency of $f = 1$ Hz, where the resistance matches the DC measured value and no signal leakage through parasitic chip capacitance is present.[16] We use a phase sensitive amplifier, which can independently measure both G_1 and G_2 by averaging out any components of the measured current which are not at the base measurement frequency f or one of its multiples. Thus the current measured with the AC voltage does contain the streaming contribution, and we obtain the total current which has two independently measured components $I_1 = G_1(P)V_{\mathrm{AC}}$ and $I_2 = G_2(P)V_{\mathrm{AC}}^2$, which are used to calculate the ICR ratio r defined in equation 1. AC measurements are performed, with high precision, to extract the linear pore resistance $R_{\mathrm{AC}} = G_1^{-1}$, and the ionic current rectification r at different pressures P (See Supporting information S2 for details).

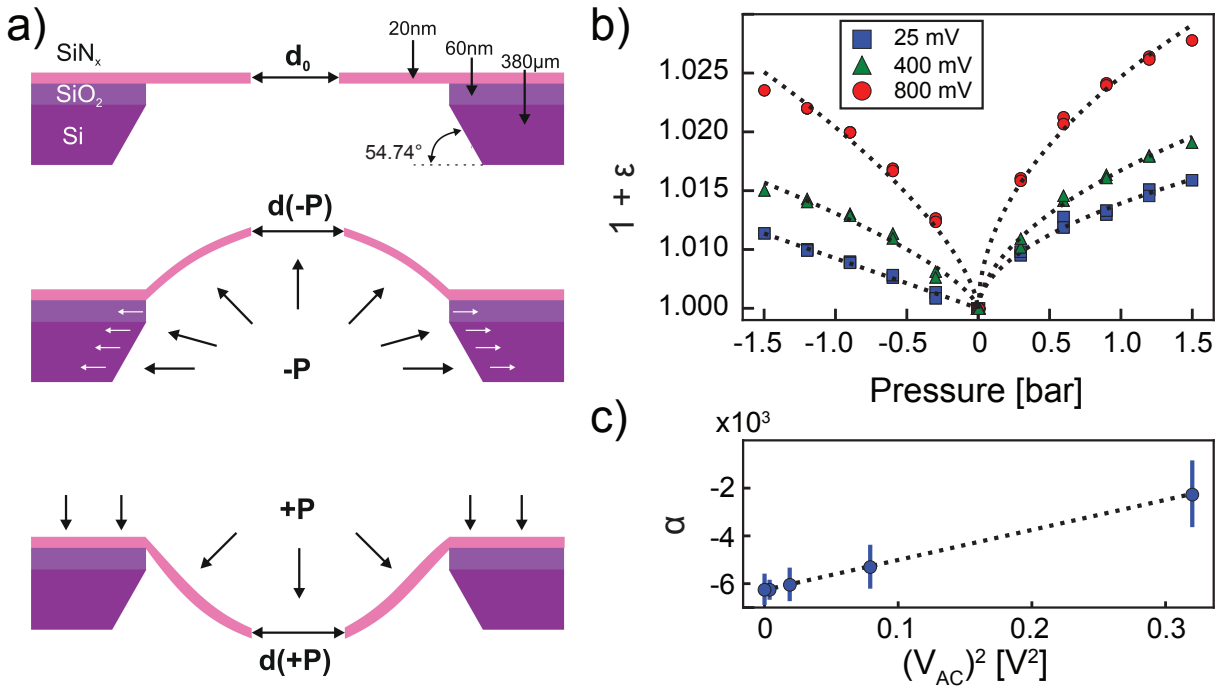

Figure 2: **Elastic response of membranes under pressure: strain induced enlargement. a)** Schematic of the chip and membrane with nanopore. The initial configuration under zero applied pressure is shown as well as two schematics showing the deformation under both positive, and negative pressure. This deformation due to strain enlarges the pore, $d(-P)$ and $d(+P)$. The negative pressure is also shown to act on the etched walls of the back-side of the chip leading to an asymmetric response. **b)** Normalised strain value as a function of pressure for the same membrane at a low bias voltage of $V_{\mathrm{AC}} = 25$ mV (blue squares), $V_{\mathrm{AC}} = 400$ mV (green triangles), and $V_0 = 800$ mV (red circles). AC voltages are given in root mean square values of the amplitude. Dashed black lines correspond to the fit of the stress to Eq. (2). For positive pressures zero pre-stress is considered while for negative pressures the full Eq. (2) is used. **c)** Voltage dependence of the residual stress factor α with a quadratic fit (dashed line). Error bars represent the standard deviation obtained from the fit.

Strain induced pore enlargement

When pressure and thus strain is applied to one side of the suspended silicon nitride membrane it blisters. Its deformation can be modelled as a thin sheet under large elastic deformations due to a uniform load in the direction perpendicular to the plane of the membrane.[38] The square membranes used are of side length $a = 10-30$ μm. The pore at the center can be treated as a perturbation which will not significantly influence the stress distribution in the membrane. Since the measured resistance R_{AC} is related to the pore diameter d, any change of resistance with pressure is related to a modification of d. The resistance decreases indepen-

dently of the direction of applied pressure (Figure 1c), and does not depend on the nanopore surface charge (Supporting Figure S6). The measured change of pore resistance R_{AC} with pressure is attributed to the local strain at the nanopore due to stress in the membrane. The stress being radially symmetric at the center of the membrane, and the elastic model involving only linear elastic deformations in the plane of the membrane, the change in size of the nanopore is trivially shown[39] to be $d(P) = d_0\,(1 + \epsilon(P))$ where $\epsilon(P) = (1 - \nu^2)\sigma_r(P)/E$ is the pressure dependent strain, σ_r is the radial stress in the membrane, and d_0 is the pore diameter under no applied stress. Thus by precisely measuring the change in the nanopore resistance, the local strain/stress at the membrane is obtained.

The elastic response of silicon nitride membranes is well studied[21,24] which allows to validate our model of pore enlargement. The elastic response will depend on the applied pressure P as well as the geometric and elastic parameters of the membrane: a the size of the square membrane, L the thickness of the membrane, E the Young's modulus, and ν the Poisson ratio. In addition, under no external pressure load, the membrane exhibits some pre-stress σ_0 acting to stretch or compress the membrane in the lateral direction. In this regime, neglecting bending, and assuming that the stress is constant over the membrane, the stress can be described by:[21]

$$\sigma_r^3 - \sigma_0\sigma_r^2 - \frac{EP^2a^2}{6L^2(1-\nu)^2} = 0. \tag{2}$$

By inserting the pressure dependent diameter $d(P)$ into the conductivity of the nanopore G_1 we are able to reproduce the dependence of the strain at the pore ϵ at different pressures. Figure 2a shows a fit of the strain ϵ measured due to nanopore enlargement at different values of the pressure difference P and applied sinusoidal voltage amplitude. The elastic parameters are taken to be $\nu = 0.23$, $L = 20$ nm, and $E = 200$ GPa, which is the average Young modulus dependent on the specifics of the fabrication procedure.[40] The positive pressure behaviour is fitted at a driving potential of 25 mV to a simplified $\sigma_0 = 0$ case, while the negative pressure

is fitted with $\sigma_0 \neq 0$. We find excellent agreement with the model for low electrical driving potentials, and membrane sizes for different samples are correctly extracted (Figure 1c).

While the prediction of the correct membrane size shows that the simplified $\sigma_0 = 0$ case is valid it is not sufficient to completely explain the asymmetry at low voltage (as seen in Figure 2b). A fit assuming a constant σ_0 in the negative pressure direction gives values of up to 1 GPa, much higher than reported values of intrinsic stress of below 500 MPa for different growth conditions,[41,42] and not supported by the low level of deformation of the membranes measured by atomic force microscopy (Supporting Figure S4). In addition, intrinsic pre-stress of the membrane would affect both the positive and negative pressure behaviour and does not explain the observed asymmetry with pressure. We propose that this is due to the back side etched cavity present on the chips (Figure 2a). Application of pressure to the back-side of the chip induces forces on the etched silicon walls inside the cavity which tends to stretch the suspended membrane and modify the pre-stress. Assuming a pressure dependent pre-stress for negative pressures of the form $\sigma_0 = \alpha P$ we find a value of $\alpha \approx -6000$ at the lowest applied sinusoidal potential (Figure 2c). This value can be rationalised from geometrical considerations. The applied pressure will induce a force $F_{in} \propto L_{\mathrm{Si}} P \sin(54, 74^\circ)$, where $L_{\mathrm{Si}} = 380$ μm is the thickness of the silicon substrate, with the angle $54, 74^\circ$ defined by crystallographic planes. This estimate gives a comparable pressure induced pre-stress factor of $\alpha \approx L_{\mathrm{Si}} \sin(54^\circ)/L \approx -10000$ while neglecting any fine effects dependent on the manufacturing process.

Although including a pressure dependent pre-stress for negative pressures explains most of the measured behaviour, Figure 2c shows that the pressure induced pre-stress factor α decreases quadratically with voltage. We propose that this effect is due to electrostriction of the underlying chip material which is known to occur for all dielectrics at high electric field regardless of crystal symmetry.[43,44] Considering the thickness of the samples, the electric field at 800 mV RMS is on the order of 2 kV/m over the silicon substrate and on the order of 40 MV/m over the 20 nm thick silicon nitride membrane, sufficient to produce several

percent of strain due to electrostriction. This electrostrictive stress counterbalances the pressure induced pre-stress discussed above returning a symmetric pressure profile at high voltage. At large voltages the measured data deviates from the model and we assume that the stresses in these cases are no longer within the range of validity of eq. 2.

Pressure induced ionic current rectification

After studying pore enlargement under pressure, we investigate how pressure modifies the non-linear conductivity of the nanopore quantified by ICR. Figure 3 shows the ICR ratio increasing with applied pressure, reaching a maximum at $P \approx 500$ mbar, and reducing with higher pressure magnitudes. The decrease in ICR with an increase in pressure is well known,[19,20,45] but to our knowledge an increase in ICR with pressure has not yet been reported. The magnitude of ICR is known to be strongly dependent on the surface charge,[5,7] so we change its value by varying the pH of the solution. The point of zero charge for silicon nitride membranes is $\approx$ pH 4.[15] Figure 3b shows how a pH larger than 8 increases the ICR magnitude due to a slight increase in surface charge while not changing the pressure dependence. Conversely going near the point of zero charge at pH 3 completely removes any pressure dependence of ICR. Here the magnitude of ICR is small as we use a high salt concentration (1 M KCl), but is expected to grow at lower concentrations due to a larger contribution from the surface double layer.[46]

To explain the origin of the pressure induced ICR, we perform finite element method (FEM) modelling in COMSOL multiphysics. Coupled Poisson-Nernst-Planck-Stokes equations are solved with static pressure between the two electrolyte reservoirs while varying the surface charge Σ, and DC voltage bias (See Supporting information Sec. S5). Considering the complete decoupling of the strain effect no change in shape of the pore due to the elastic deformations is considered. Figure 3c shows FEM values of rectification based on eq. 1 as a function of pressure for three surface charge values chosen to simulate the effect of exper-

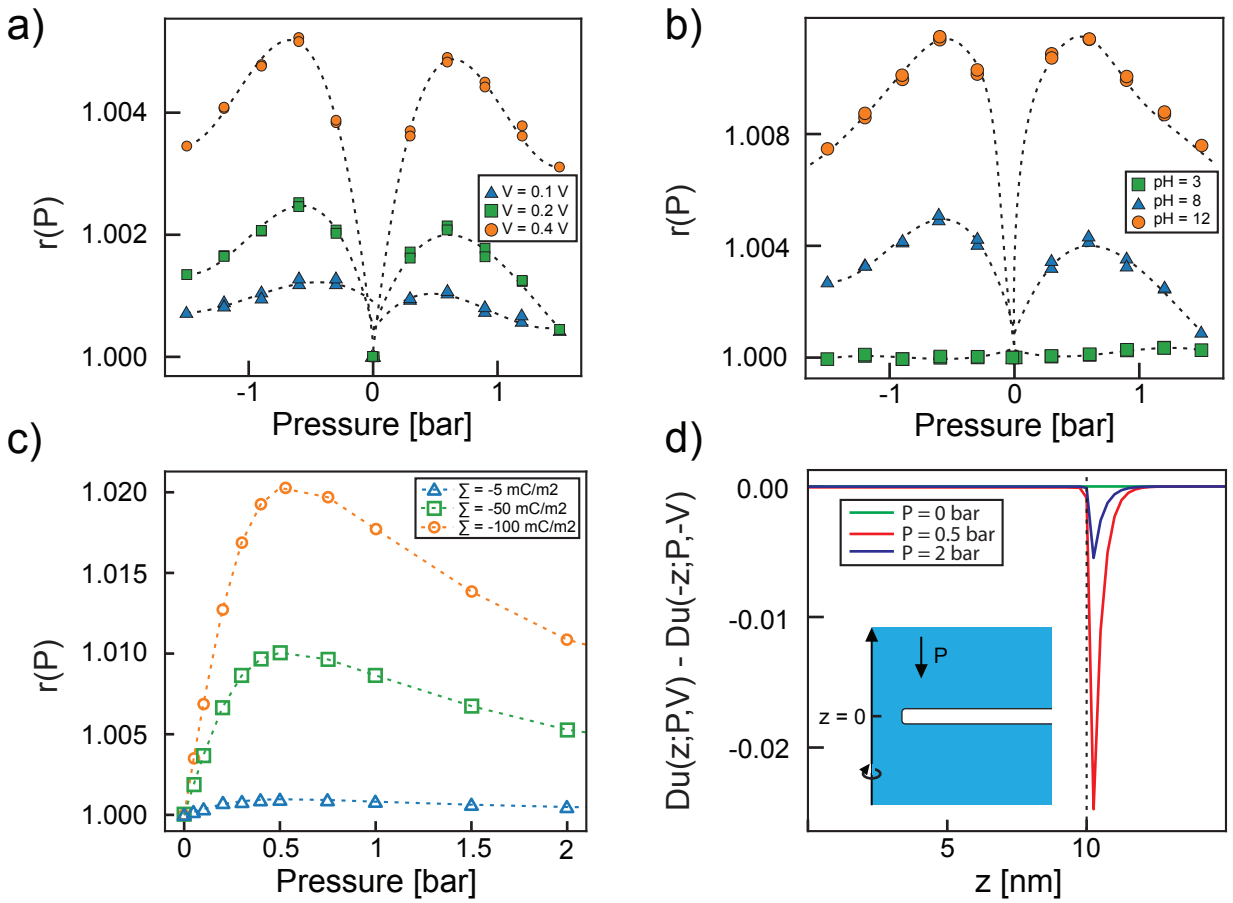

Figure 3: **Pressure-induced rectification in symmetric solid state nanopores. a)** Rectification r as a function of pressure P for different driving voltages V_{AC}. Rectification values are corrected for baseline drift and offsets as described in the Materials and Methods. **b)** Measured rectification for three different pH values (i.e different surface charge densities). Corresponding streaming current measurements are provided on Supporting Figure S5. **c)** Rectification extracted from COMSOL model of a solid state nanopore under pressure. Surface charges of $\Sigma = -5$ mC/m^2, -50 mC/m^2, and -100 mC/m^2 are chosen to simulate the pH 3, 8, and 12 case respectively. **d)** Spatial asymmetry in the Dukhin number for positive and negative bias $\mathrm{Du}(z;P,V) - \mathrm{Du}(-z;P,-V)$ along the pore axis. Three representative pressures are shown: $P = 0$, approximate maximum in ICR $P = 0.5$ bar, and region of ICR reduction with pressure $P = 2$ bar. Inset shows the radially symmetric FEM simulation geometry, pressure direction, and z axis.

imental pH changes. Only positive pressure gradients are shown since the measurement is by definition symmetric in pressure. The FEM model completely captures the behaviour seen in the experimental data on Figure 3b, with an increase in r at low pressures before a turnover and decrease at higher pressures. The measured decrease in magnitude of the effect as the surface charge is reduced is also captured.

The rectification behaviour can be rationalised in terms of perturbations to the ion distributions in and around the nanopore caused by pressure-induced advection. ICR in nanapores has been shown to be controlled by the spatial variation in the axial direction z of the local Dukhin number $\mathrm{Du}(z)$, with stronger asymmetry of $\mathrm{Du}(z)$ between the pore ends yielding stronger rectification.[7] The Dukhin number measures the relative magnitude of surface to bulk ionic conduction. For a 1:1 electrolyte, and in the absence of Debye layer overlap, $\mathrm{Du}(z) = -\frac{\langle c_+(z) - c_-(z)\rangle}{2(c_+(z,r=0)+c_-(z,r=0))}$, where $c_\pm$ are the positive and negative ion concentrations, $\langle \cdots \rangle$ denotes an average over the pore cross-section, and r is the radial coordinate.[7] Pressure-driven flow induces spatial asymmetry in $\mathrm{Du}(z)$ since conservation of ion current as the bulk solution is transported into the charged nanopore perturbs both the local ionic charge density $n_c = e(c_+ - c_-)$, and local total ion concentration $c_{\mathrm{tot}} = c_+ + c_-$ (Supplemental Figures S8 and S9 respectively), particularly when coupled with the applied electric field. At sufficiently high pressures, however, advection completely replaces the fluid inside the nanopore with bulk solution, reducing the spatial variation of $\mathrm{Du}(z)$ and diminishing ICR, as observed in both experiments and FEM simulations. The spatial asymmetry of $\mathrm{Du}(z)$ at positive versus negative bias $\pm V$ for different pressures P from the FEM simulations is quantified by $\mathrm{Du}(z; P, V) - \mathrm{Du}(-z; P, -V)$ in Figure 3d, which confirms that the asymmetry is greatest at intermediate pressure corresponding to the strongest ICR. In this case of a high salt concentration the absolute value of the Dukhin number is small $\mathrm{Du} \approx 0.013$, however, asymmetry in Dukhin number is still large enough to drive the effect which is expected to grow as the salt concentration decreases.

The pressure-induced asymmetry in $\mathrm{Du}(z)$ is localized to the pore ends in the FEM sim-

ulations (Figure 3d). Thus, rectification is expected to be controlled by a Péclet number $\mathrm{Pe} = \frac{ud}{D}$ quantifying the relative importance of advection to diffusion in which the characteristic length scale is the pore diameter d. Here, u is the average pressure-driven fluid velocity and D the diffusivity of the ions (which is approximately the same for K^+ and Cl^-). ICR is expected to be pronounced for $\mathrm{Pe} > 1$ and to diminish as $\mathrm{Pe} \to \infty$. Consistent with this picture, the maximum ICR in the experiments and FEM simulations (at $P \approx 500$ mbar) occurs at $\mathrm{Pe} \approx 7$, if we take $u \approx \frac{d^2 P}{2\eta(16L+3\pi d)}$,[47] the average fluid velocity magnitude across a nanopore of length L and diameter d for fluid viscosity η due to an applied pressure P and use the experimental/simulation parameter values.

Conclusions

By coupling a perfectly wetted nanopore inside a thin elastic silicon nitride membrane, we demonstrated how AC measurements of ion transport coupled with hydrostatic pressure precisely measure two separate physical phenomena. By monitoring the size of the nanopore while the membrane is undergoing pressure induced blistering, we demonstrate that local strain in the membrane can be accurately measured. As these membranes are typically used as supports for 2D material nanopore measurements, this is the first step to measuring mechanosensitivity in 2D materials[28–32] as it allows calibration and controlled application of stresses. Stress in the 2D membrane under deformation is expected to cause restructuring of bonds in the nanopore edges, opening up pathways for ion transport, in direct analogy to biological ion channels.[33] This could provide a stress-sensitive alternative to the newly reported pressure sensitive ion transport behaviour in single digit carbon nanotubes.[18] In addition to strain induced enlargement of nanopores, we have shown how thin symmetric nanopores under pressure exhibit non-linear transport phenomena such as ICR. This is in contrast to the so far reported effect of the reduction of ICR with pressure.[19,20] Similar to systems which have liquid flow slippage, like long carbon nanotubes,[18] or angstrom slits,[17]

membranes in almost-2D membranes have low hydraulic resistance which, along with access effects, produces novel non-linear nanofluidic phenomena.

Supporting information

The supporting information contains the Materials and methods section, details about the strain and ionic current rectification measurements, and FEM model details with additional plots.

Author contributions

S.J.D. performed the experiments, analysed the data, and performed FEM simulations. S.M. designed and built the experimental set-up, and built the FEM model. M.M. designed the microfluidic chamber, and performed AFM imaging. A.C. fabricated devices. A.R. and S.M. supervised the research. D.M.H. provided an explanation for the ionic current rectification. S.J.D. and S.M. wrote the manuscript with all authors providing important suggestions for the experiments, discussing the results, and contributing to the manuscript.

Acknowledgement

The authors thank Marko Popovic and Alex Smolyanitsky for useful discussions on the membrane elasticity. This work was financially supported by the Swiss National Science Foundation (SNSF) Consolidator grant (BIONIC BSCGI0_157802) and from the European Union's Horizon 2020 research and innovation programme under the Marie SkÅĆodowska-Curie grant agreement No 754462.

References

1. Plesa, C.; Kowalczyk, S. W.; Zinsmeester, R.; Grosberg, A. Y.; Rabin, Y.; Dekker, C. Fast Translocation of Proteins through Solid State Nanopores. *Nano Lett.* **2013**, *13*, 658–663.

2. Merchant, C. A.; Healy, K.; Wanunu, M.; Ray, V.; Peterman, N.; Bartel, J.; Fischbein, M. D.; Venta, K.; Luo, Z.; Johnson, A. T. C. *et al.* DNA Translocation through Graphene Nanopores. *Nano Lett.* **2010**, *10*, 2915–2921.

3. Macha, M.; Marion, S.; Nandigana, V. V. R.; Radenovic, A. 2D materials as an emerging platform for nanopore-based power generation. *Nat. Rev. Mater.* **2019**, *4*, 588–605.

4. Epsztein, R.; DuChanois, R. M.; Ritt, C. L.; Noy, A.; Elimelech, M. Towards single-species selectivity of membranes with subnanometre pores. *Nat. Nanotechnol.* **2020**,

5. Siwy, Z. Ion-Current Rectification in Nanopores and Nanotubes with Broken Symmetry. *Adv. Funct. Mater.* **2006**, *16*, 735–746.

6. Gravelle, S.; Ybert, C. Flow-induced shift of the Donnan equilibrium for ultra-sensitive mass transport measurement through a single nanochannel. *J. Chem. Phys.* **2019**, *151*, 244503.

7. Poggioli, A. R.; Siria, A.; Bocquet, L. Beyond the Tradeoff: Dynamic Selectivity in Ionic Transport and Current Rectification. *J. Phys. Chem. B* **2019**, *123*, 1171–1185.

8. Bocquet, L.; Charlaix, E. Nanofluidics, from bulk to interfaces. *Chem. Soc. Rev.* **2010**, *39*, 1073–1095.

9. Graf, M.; Lihter, M.; Thakur, M.; Georgiou, V.; Topolancik, J.; Ilic, B. R.; Liu, K.; Feng, J.; Astier, Y.; Radenovic, A. Fabrication and practical applications of molybdenum disulfide nanopores. *Nat. Protoc.* **2019**, *14*, 1130–1168.

10. Thakur, M.; Macha, M.; Chernev, A.; Graf, M.; Lihter, M.; Deen, J.; Tripathi, M.; Kis, A.; Radenovic, A. Wafer-Scale Fabrication of Nanopore Devices for Single-Molecule DNA Biosensing using MoS2. *Small Methods* **2020**, *n/a*, 2000072.

11. Zhang, H.; Zhao, Q.; Tang, Z.; Liu, S.; Li, Q.; Fan, Z.; Yang, F.; You, L.; Li, X.; Zhang, J. *et al.* Slowing Down DNA Translocation Through Solid-State Nanopores by Pressure. *Small* **2013**, *9*, 4112–4117.

12. Lu, B.; Hoogerheide, D. P.; Zhao, Q.; Zhang, H.; Tang, Z.; Yu, D.; Golovchenko, J. A. Pressure-Controlled Motion of Single Polymers through Solid-State Nanopores. *Nano Lett.* **2013**, *13*, 3048–3052.

13. Li, J.; Hu, R.; Li, X.; Tong, X.; Yu, D.; Zhao, Q. Tiny Protein Detection Using Pressure through Solid-State Nanopores. *Electrophoresis* **2017**, *38*.

14. Hoogerheide, D. P.; Lu, B.; Golovchenko, J. A. Pressure-Voltage Trap for DNA near a Solid-State Nanopore. *ACS Nano* **2014**, *8*, 7384–7391.

15. Firnkes, M.; Pedone, D.; Knezevic, J.; Doblinger, M.; Rant, U. Electrically Facilitated Translocations of Proteins through Silicon Nitride Nanopores: Conjoint and Competitive Action of Diffusion, Electrophoresis, and Electroosmosis. *Nano Lett.* **2010**, *10*, 2162–2167.

16. Marion, S.; Macha, M.; Davis, S. J.; Chernev, A.; Radenovic, A. Wetting of nanopores probed with pressure. 2019; 1911.05229, arxiv, `https://arxiv.org/abs/1911.05229` accessed 09.30.2020.

17. Mouterde, T.; Keerthi, A.; Poggioli, A. R.; Dar, S. A.; Siria, A.; Geim, A. K.; Bocquet, L.; Radha, B. Molecular streaming and its voltage control in ångström-scale channels. *Nature* **2019**, *567*, 87–90.

18. Marcotte, A.; Mouterde, T.; NiguÃĺs, A.; Siria, A.; Bocquet, L. Mechanically activated ionic transport across single digit carbon nanotubes. *Nat. Mater.* **2020**,

19. Lan, W.-J.; Holden, D. A.; White, H. S. Pressure-Dependent Ion Current Rectification in Conical-Shaped Glass Nanopores. *J. Am. Chem. Soc.* **2011**, *133*, 13300–13303.

20. Jubin, L.; Poggioli, A.; Siria, A.; Bocquet, L. Dramatic pressure-sensitive ion conduction in conical nanopores. *Proc. Natl. Acad. Sci. U.S.A.* **2018**, *115*, 4063–4068.

21. Vlassak, J.; Nix, W. A new bulge test technique for the determination of Young's modulus and Poisson's ratio of thin films. *J. Mater. Res.* **1992**, *7*, 3242–3249.

22. Koenig, S. P.; Boddeti, N. G.; Dunn, M. L.; Bunch, J. S. Ultrastrong adhesion of graphene membranes. *Nat. Nanotechnol.* **2011**, *6*, 543–546.

23. Boddeti, N. G.; Liu, X.; Long, R.; Xiao, J.; Bunch, J. S.; Dunn, M. L. Graphene Blisters with Switchable Shapes Controlled by Pressure and Adhesion. *Nano Lett.* **2013**, *13*, 6216–6221.

24. Bunch, J. S.; Verbridge, S. S.; Alden, J. S.; van der Zande, A. M.; Parpia, J. M.; Craighead, H. G.; McEuen, P. L. Impermeable Atomic Membranes from Graphene Sheets. *Nano Lett.* **2008**, *8*, 2458–2462.

25. Willmott, G. R.; Moore, P. W. Reversible mechanical actuation of elastomeric nanopores. *Nanotechnology* **2008**, *19*, 475504.

26. Roberts, G. S.; Kozak, D.; Anderson, W.; Broom, M. F.; Vogel, R.; Trau, M. Tunable Nano/Micropores for Particle Detection and Discrimination: Scanning Ion Occlusion Spectroscopy. *Small* **2010**, *6*, 2653–2658.

27. Humplik, T.; Lee, J.; O'Hern, S. C.; Fellman, B. A.; Baig, M. A.; Hassan, S. F.; Atieh, M. A.; Rahman, F.; Laoui, T.; Karnik, R. *et al.* Nanostructured materials for water desalination. *Nanotechnology* **2011**, *22*, 292001.

28. Li, W.; Yang, Y.; Weber, J. K.; Zhang, G.; Zhou, R. Tunable, Strain-Controlled Nanoporous MoS2 Filter for Water Desalination. *ACS Nano* **2016**, *10*, 1829–1835.

29. Fang, A.; Kroenlein, K.; Smolyanitsky, A. Mechanosensitive Ion Permeation across Subnanoporous MoS2 Monolayers. *J. Phys. Chem. C* **2019**, *123*, 3588–3593.

30. Sahu, S.; Elenewski, J.; Rohmann, C.; Zwolak, M. Optimal transport and colossal ionic mechano-conductance in graphene crown ethers. *Sci. Adv.* **2019**, *5*.

31. Fang, A.; Kroenlein, K.; Riccardi, D.; Smolyanitsky, A. Highly mechanosensitive ion channels from graphene-embedded crown ethers. *Nat. Mater.* **2019**, *18*, 76–81.

32. Smolyanitsky, A.; Fang, A.; Kazakov, A. F.; Paulechka, E. Ion transport across solid-state ion channels perturbed by directed strain. *Nanoscale* **2020**, *12*, 10328–10334.

33. Biophysical Principles of Ion-Channel-Mediated Mechanosensory Transduction. *Cell Rep.* **2019**, *29*, 1–12.

34. Rabinowitz, J.; Edwards, M. A.; Whittier, E.; Jayant, K.; Shepard, K. L. Nanoscale Fluid Vortices and Nonlinear Electroosmotic Flow Drive Ion Current Rectification in the Presence of Concentration Gradients. *The Journal of Physical Chemistry A* **2019**, *123*, 8285–8293.

35. Qiu, Y.; Siwy, Z. S.; Wanunu, M. Abnormal Ionic-Current Rectification Caused by Reversed Electroosmotic Flow under Viscosity Gradients across Thin Nanopores. *Analytical Chemistry* **2019**, *91*, 996–1004.

36. Hall, J. E. Access resistance of a small circular pore. *J. Gen. Physiol.* **1975**, *66*, 531–532.

37. Kowalczyk, S. W.; Grosberg, A. Y.; Rabin, Y.; Dekker, C. Modeling the conductance and DNA blockade of solid-state nanopores. *Nanotechnology* **2011**, *22*, 315101.

38. Timoshenko, S. P.; Woinowsky-Krieger, S. *Theory of Plates and Shells*; McGraw-Hill, New York, 1959.

39. Dye, N. A.; Popovic, M.; Iyer, K. V.; Eaton, S.; Julicher, F. Self-organized patterning of cell morphology via mechanosensitive feedback. 2020; 2020.04.16.044883, bioarxiv, `https://www.biorxiv.org/content/early/2020/04/18/2020.04.16.044883` accessed 09.30.2020.

40. Buchaillot, L.; Farnault, E.; Hoummady, M.; Fujita, H. Silicon Nitride Thin Films Young's Modulus Determination by an Optical Non Destructive Method. *Jpn. J. Appl. Phys.* **1997**, *36*, L794–L797.

41. Temple-Boyer, P.; Rossi, C.; Saint-Etienne, E.; Scheid, E. Residual stress in low pressure chemical vapor deposition SiNx films deposited from silane and ammonia. *J. Vac. Sci. Technol. A* **1998**, *16*, 2003–2007.

42. Noskov, A.; Gorokhov, E.; Sokolova, G.; Trukhanov, E.; Stenin, S. Correlation between stress and structure in chemically vapour deposited silicon nitride films. *Thin Solid Films* **1988**, *162*, 129 – 143.

43. van Sterkenburg, S. W. P. The electrostriction of silicon and diamond. *J. Phys. D: Appl. Phys* **1992**, *25*, 996–1003.

44. Blaffart, F.; Van Overmeere, Q.; Pardoen, T.; Proost, J. In situ monitoring of electrostriction in anodic and thermal silicon dioxide thin films. *J. Solid State Electr.* **2013**, *17*, 1945–1954.

45. Lan, W.-J.; Edwards, M. A.; Luo, L.; Perera, R. T.; Wu, X.; Martin, C. R.; White, H. S. Voltage-Rectified Current and Fluid Flow in Conical Nanopores. *Acc. Chem. Res.* **2016**, *49*, 2605–2613.

46. Lee, C.; Joly, L.; Siria, A.; Biance, A.-L.; Fulcrand, R.; Bocquet, L. Large Apparent Electric Size of Solid-State Nanopores Due to Spatially Extended Surface Conduction. *Nano Lett.* **2012**, *12*, 4037–4044.

47. Weissberg, H. L. End Correction for Slow Viscous Flow through Long Tubes. *Phys. Fluids* **1962**, *5*, 1033–1036.